Tatiana K. Dobroserdova*, Yuri V. Vassilevski, Sergey S. Simakov, Timur M. Gamilov, Andrey A. Svobodov, and Lyudmila A. Yurpolskaya

Two-scale haemodynamic modelling for patients with Fontan circulation

https://doi.org/10.1515/rnam-2021-0022
Received April 30, 2021; revised July 12, 2021; accepted August 17, 2021

Abstract: Palliation of congenital single ventricle heart defects suggests multi-stage surgical interventions that divert blood flow from the inferior and superior vena cava directly to the right and left pulmonary arteries, skipping the right ventricle. Such system with cavopulmonary anastomoses and single left ventricle is called Fontan circulation, and the region of reconnection is called the total cavopulmonary connection (TCPC). Computational blood flow models allow clinicians to predict the results of the Fontan operation, to choose an optimal configuration of TCPC and thus to reduce negative postoperative consequences. We propose a two-scale (1D3D) haemodynamic model of systemic circulation for a patient who has underwent Fontan surgical operation. We use CT and 4D flow MRI data to personalize the model. The model is tuned to patient's data and is able to represent measured time-averaged flow rates at the inlets and outlets of TCPC, as well as pressure in TCPC for the patient in horizontal position. We demonstrate that changing to quiescent standing position leads to other patterns of blood flow in regional (TCPC) and global haemodynamics. This confirms clinical data on exercise intolerance of Fontan patients.

Keywords: Fontan circulation, haemodynamics, boundary conditions, TCPC, multiscale model.

MSC 2010: 76-10

Congenital single ventricle heart defects require multi-stage surgical interventions for palliation. As the result, blood from the inferior and superior vena cava (IVC and SVC) passes the right ventricle and flows directly to the right and left pulmonary arteries (RPA and LPA). Such system with cavopulmonary anastomoses and single left ventricle is called Fontan circulation, and the region of reconnection is called the total cavopulmonary connection (TCPC). Among several possible palliative strategies, the bidirectional cava-pulmonary anastomosis (BCPA) with extracardiac conduit technique is considered to be one of the most popular and safe [15]. Even the best solution may have long-term complications originating from haemodynamic disorders [8, 15]:

- low wall shear stress (WSS) in TCPC leads to thrombosis and thromboembolism;
- high WSS in TCPC and unbalanced blood distribution between RPA and LPA lead to pulmonary arteriovenous malformations;
- fenestrations and venoarterial discharge lead to arterial hypoxemia;
- intraoperative damage of the cardiac conduction system leads to arrhythmias;
- high central venous and lymphatic pressure lead to liver dysfunction, plastic bronchitis, protein-losing enteropathy;

***Corresponding author: Tatiana K. Dobroserdova,** Marchuk Institute of Numerical Mathematics, Russian Academy of Sciences, Moscow 119333, Russia. E-mail: dobroserdovatk@gmail.com
Yuri V. Vassilevski, Sergey S. Simakov, Marchuk Institute of Numerical Mathematics, Russian Academy of Sciences, Moscow 119333, Russia; Moscow Institute of Physics and Technology, Dolgoprydny 141701, Russia; Sechenov University, Moscow 119991, Russia
Timur M. Gamilov, Marchuk Institute of Numerical Mathematics, Russian Academy of Sciences, Moscow 119333, Russia; Moscow Institute of Physics and Technology, Dolgoprydny 141701, Russia; World–Class Research Center 'Digital biodesign and personalized healthcare', Sechenov University, Moscow 119991, Russia
Andrey A. Svobodov, Lyudmila A. Yurpolskaya, Bakulev Scientific Center of Cardiovascular Surgery, Moscow 121552, Russia

- decreased left ventricular ejection fraction leads to circulatory failure;
- narrowed bulboventricular foramen leads to subaortic obstruction;
- energy loss in TCPC, high pulmonary and TCPC resistances lead to exercise intolerance.

Patients with Fontan circulation typically have high central venous pressure, low trans-pulmonary gradients and a limited preload [21, 24]. Most of haemodynamic disorders are associated with the geometry of TCPC and therefore may be predicted and minimized with blood flow simulations in TCPC as most approaches do. An optimal surgical decision

- minimizes pulmonary and TCPC resistances;
- minimizes energy dissipation in TCPC;
- balances the hepatic flow distribution (HFD) between the right and left lungs;
- does not produce regions with too high or too low WSS.

Sometimes different decisions optimize different control indicators, and clinician's choice is based on the whole patient's data and anamnesis [21]. A normalization of haemodynamic metrics which removes confounding effects is not yet elaborated [24].

Computational blood flow models allow clinicians to predict the results of the Fontan operation, to choose an optimal configuration of TCPC and thus to reduce negative postoperative consequences. This is particularly important for patients with unusual anatomic configurations who cannot rely on surgeon's experience. Several research groups have developed approaches based on 3D blood flow models for postoperative prediction [1, 4, 11, 21, 24]. The preoperative 3D vascular geometry is usually recovered from CT or MRI images. Doppler examination, 4D flow MRI data, pressure measurements are used for prescribing patient-specific boundary conditions and tuning model parameters. The 3D blood flow is computed by the numerical solution of the Navier–Stokes equations. Surgical techniques can be accounted for in the model in order to predict postoperative outcomes. The optimal technique of surgery and/or TCPC geometry are chosen according to the computed control indicators.

However, the common assumption of local haemodynamic models that postoperative inflow and outflow boundary conditions are the same as preoperative, is not correct [1]: blood redistribution causes significant changes of flow rate waveforms. Moreover, local haemodynamic models cannot take into account comorbidities and changes in the global circulation, cannot estimate postoperative central venous pressure, haemodynamic redistribution during exercises, haemodynamic changes in the heart such as increased left ventricle afterload, left atrium pressure, arrhythmias, decreased ventricular ejection fraction.

For these purposes models of global circulation should be used. A closed loop lumped parameter model was applied for investigation of exercise physiology in Fontan patients in [12]. In [1] a global multiscale haemodynamic model for a Fontan patient was based on a lumped parameter model of the entire cardiovascular system coupled with a 3D patient-specific model of BCPA or TCPC representing the detailed pulmonary anatomy. The model confirms that recovery of postoperative flow waveforms is impossible if inflow changes are neglected. Personalization of the global lumped parameter model is difficult since the electrical circuit parameters of the model do not correspond directly to haemodynamic measurements. One-dimensional (1D) haemodynamic models are personalized more naturally [23] and applied for many medical applications as they account for various comorbidities beyond the TCPC region (stenoses, aneurysms, subaortic obstruction etc.), external influences (gravity, autoregulation), exercise stress. Moreover, such models can take aging into account by scaling vessel sizes and changing elastic vessel wall properties according to the age [23]. This is particularly important for patients with Fontan circulation: many complications appear several years after the surgical intervention, some complications correlate with the patient's age at the moment of operation. A combination of 1D and 3D haemodynamic models defines a two-scale model of the full Fontan circulation which provides correct upstream boundary conditions for the TCPC region depending on various factors and monitors global haemodynamics of the patient.

In the present paper we develop a new two-scale 1D3D model for a patient with Fontan circulation. TCPC region is represented by a 3D domain and the remaining part of the systemic circulation is represented by a 1D graph. The inflow boundary condition is based on 4D flow MRI data. The 1D model of the systemic

circulation [16, 23], geometry of 3D domain and the outflow boundary conditions for pulmonary arteries are tuned according to patient-specific data. We adopt the 1D3D two-scale model to known haemodynamics of the patient with Fontan circulation in horizontal position and then apply it for the same patient in quiescent standing position. The comparison of simulations in different positions allows us to analyze changes of blood flow and inflow rates in TCPC as well as global haemodynamic indices such as the central venous pressure, the arterial pressure, etc. In particular, changes of the hepatic circulation can be assessed directly in contrast to indirect HFD analysis. In future the developed model can predict surgical Fontan operations and provide more control indicators determining the operation outcomes.

The rest of the paper is organized as follows. In Section 1 we present and analyze medical data for the patient. In Section 2 we introduce the two-scale haemodynamic model and in Section 3 we discuss its personalization. In Section 4 we apply the model to the haemodynamic analysis of the Fontan patient in horizontal and standing positions. Section 5 collects the final remarks and conclusions.

1 Splendour and misery of medical data

Patients undergo medical examination before and after the Fontan operation. Anthropometric measurements (height, weight), tonometric measurement (arm pressure), ultrasound scanning are available for every patient. For certain Fontan patients, invasive measurements (catheterized pressure in veins) are taken as well.

Chest CT and/or MRI with 4D flow data are advanced options of medical examination. Usually mathematical models rely on flow data in the systemic veins and pulmonary arteries in the vicinity of TCPC, but the same data is also available for the aortic arch and can be applied in the model. MRI 4D flow data provide flow rates, velocities and vascular cross-section areas during the cardiac cycle in sections of interest. Although such data are very attractive for numerical simulations, we do not recommend their straightforward using in personalized models for the following reasons.

We have analyzed data of a patient with congenital heart disease who underwent two surgical operations. SVC and RPA were connected at the age of 3 years during the first stage (BCPC). The Fontan operation was performed at the age of 12 years, when the extracardiac conduit between IVC and LPA was implanted (TCPC). MRI examination was done using Siemens Avanto 1.5T scanner 1.5 years later, when the patient was 14 years old. MRI 4D flow data were recovered in several cross-sections of aorta, SVC, IVC, RPA, LPA shown in Fig. 1. Table 1 collects time-averaged flow rates and lumen areas corresponding to these cross-sections.

Cross-sections 2 and 3 of TCPC (see Fig. 1b) belong to the conduit, cross-section 1 belongs to the IVC or the conduit. Since the conduit material is not extendable in the conduit cross-section, the lumen area should be constant in time. The shape of the conduit assumes that areas of cross-sections 2 and 3 should be equal. However, the MRI 4D flow data provide essentially different areas, 94.0 and 124.3 mm^2, respectively (see Table 1). Moreover, within the cardiac cycle the MRI-based areas vary between 84.7 and 101.2 mm^2 (cross-section 2), and between 113.7 and 135.9 mm^2 (cross-section 3). The cross-section area may be estimated by an

Tab. 1: MRI 4D flow data of the patient: time-averaged flow rates Q_{av} and lumen areas S_{av} in cross-sections of the aorta and TCPC. Indices of the cross-sections are shown in Fig. 1.

Aorta				TCPC			
Cross-section	Vessel name	Q_{av} (mL/sec)	S_{av} (mm^2)	Cross-section	Vessel name	Q_{av} (mL/sec)	S_{av} (mm^2)
3	Aorta	41.6	290.3	1	Conduit/IVC	15.9	75.9
4	Aorta	43.6	398.8	2	Conduit	11.9	94.0
5	Aorta	24.8	182.7	3	Conduit	12.6	124.3
6	Aorta	21.0	150.9	4	SVC	13.0	96.9
7	Aorta	24.4	182.3	5	LPA	13.8	86.1
8	Aorta	16.4	184.9	6	RPA	15.4	65.2

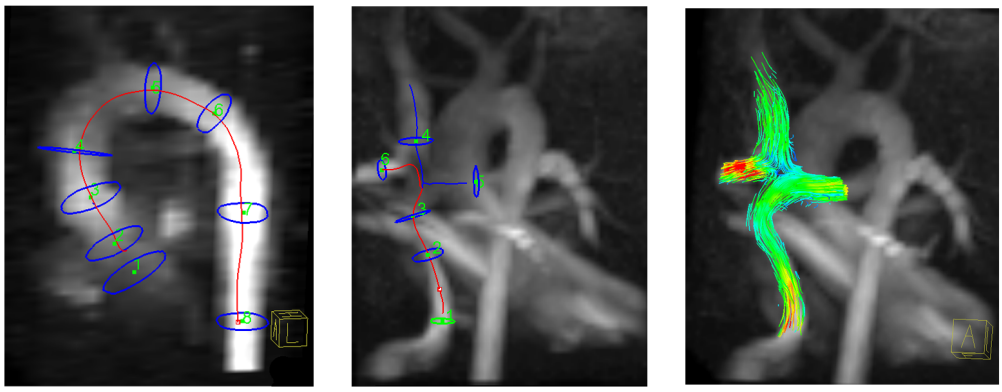

Fig. 1: Cross-sections of 4D flow MRI data for the aorta (a) and TCPC (b), velocity streamlines in TCPC (c). For TCPC, cross-section 1 is located in the conduit or IVC, cross-sections 2, 3 are in the conduit, cross-section 4 is in the SVC, cross-section 5 is in the LPA, cross-section 6 is in the RPA.

alternative method based on analysis of cine MR images. According to this method, the area of cross-section 2 varies in time between 235 and 240 mm^2 that perfectly matches the ground truth lumen conduit area.

Therefore, the MRI 4D flow data underestimate the conduit lumen considerably. One of the reasons is that the conduit diameter is chosen larger than necessary for the patient at the moment of operation accounting patient's growth, and the blood velocity is smaller in the conduit which leads to the MRI-area underestimation. Thus, CT data give more reliable geometrical parameters of the TCPC region and may be obtained almost instantly.

As concerns the flow rates, the MRI 4D flow data show that the flow in the implanted conduit pulsates. However, catheterized measurements of the blood pressure in TCPC for Fontan patients usually show values almost constant in time. Moreover, the MRI 4D flow data do not obey the conservation of mass. Indeed, the sum of time-averaged flow rates in cross-sections around TCPC, should be equal to 0. The sum of the outflow rates in cross-sections 5 and 6 is 29.2 ml/sec, whereas the sum of the inflow rates in cross-sections 4 and 1 is 28.9 ml/sec. The flow rates in cross-sections 1 and 2 of TCPC mismatch dramatically: 15.9 versus 11.9 ml/sec (see Table 1). Aorta time-averaged outflow should be equal to the averaged flow rate passing TCPC, but this is not the case in Table 1: 41.6 ml/sec in cross-section 3 of the aorta is not equal to 29.2 ml/sec in TCPC. We note that MRI velocity measurements are prone to large noise due to physics of MRI measurements [2, 6]: the noise level is 15% of the maximum measured velocity, which means the flow rate noise for data in Table 1 is at least 6 ml/sec. For aorta cross-sections 3, 4 the flow rate noise remains 15%, for the TCPC cross-sections the flow rate noise achieves 40%.

Our simulations use profile of MRI-based flow rate in the aorta cross-section. MRI-based cross-section areas are not used directly in the simulations. MRI-based time-averaged flow rates in IVC, SVC, RPA, LPA and aorta are used for scaling of the aortic flow rate and tuning model parameters (resistances of the pulmonary and systemic microvascular bed). Time-averaging reduces the noise of the measurements.

2 Two-scale haemodynamic model

The two-scale haemodynamic model is denoted by 1D3D as it couples 1D and 3D blood flow models. The blood is assumed to be viscous incompressible fluid with viscosity $\nu = 0.04\ cm^2 s^{-1}$ and density $\rho = 1\ g/cm^3$. The 3D model considers the TCPC domain as a 3D domain Ω with boundary $\partial\Omega$ composed from rigid walls Γ_0 and inlets/outlets $\Gamma_{in/out}$. Given the initial condition $\mathbf{u} = \mathbf{u}_0$ ($\operatorname{div} \mathbf{u}_0 = 0$) for $t = 0$, the blood flow in Ω is described

by the Navier–Stokes equations:

$$\rho\left(\frac{\partial \mathbf{u}}{\partial t}+(\mathbf{u}\cdot\nabla)\,\mathbf{u}\right)-\nu\Delta\mathbf{u}+\nabla p=\mathbf{f}$$
$$\operatorname{div}\mathbf{u}=0 \quad \text{in } \Omega$$
$$\mathbf{u}=\mathbf{0} \quad \text{on } \Gamma_0$$
$$\nu\frac{\partial \mathbf{u}}{\partial \mathbf{n}}-p\mathbf{n}=\gamma\mathbf{n} \quad \text{on } \Gamma_{\text{in/out}} \tag{2.1}$$

where p is the pressure, $\mathbf{u}$ is the velocity vector field, $\mathbf{n}$ is the outward normal vector, $\mathbf{f}$ is an external force, e.g., the gravity force. On rigid walls we assume no-slip and no-penetration boundary condition. At the outlets the Poiseuille's pressure drop condition is prescribed:

$$\gamma=p_{\text{out}}+R\int\limits_{\Gamma_{\text{out}}}\mathbf{u}(t,\mathbf{x})\cdot\mathbf{n}\mathrm{d}\mathbf{s} \tag{2.2}$$

where R is the hydraulic resistance for each outlet, p_{out} is the external pressure. LBB-stable Taylor–Hood (P2/P1) finite element and backward Euler time stepping are used for the approximate solution of equations (2.1).

The 1D blood flow model operates with pressure $\bar{p}$ and axial velocity $\bar{u}$ averaged over cross-sections (with area S) of a vessel with length b represented by a 1D elastic tube. The model consists of the mass balance equation, the momentum equation, and the tube law for the transmural pressure $\bar{p}-p_{\text{ext}}$:

$$\begin{cases}\dfrac{\partial S}{\partial t}+\dfrac{\partial(S\bar{u})}{\partial x}=0\\ \dfrac{\partial \bar{u}}{\partial t}+\dfrac{\partial(\bar{u}^2/2+\bar{p}/\rho)}{\partial x}=\psi(t,x,S,\bar{u}), \qquad \text{for } x\in(0,b).\\ \bar{p}-p_{\text{ext}}=\rho_w c_w^2 f(\widetilde{S})\end{cases} \tag{2.3}$$

Here $\psi(t,x,S,\bar{u})$ is an external force, e.g., the gravity and/or friction force, p_{ext} is the external pressure of surrounding tissues, where $\widetilde{S}=\widehat{S}^{-1}S$, $\widehat{S}$ is the reference area corresponding to zero transmural pressure. The third equation in (2.3) defines elastic properties of the vessel wall, ρ_w is the wall density, c_w is the velocity of wave propagation in the wall, and function f is defined as follows [16, 23]:

$$f(\widetilde{S})=\begin{cases}\exp(\widetilde{S}-1)-1, & \widetilde{S}>1\\ \ln\widetilde{S}, & \widetilde{S}\leqslant 1.\end{cases} \tag{2.4}$$

The initial conditions are $\bar{u}|_{t=0}=\bar{u}_0$, $S|_{t=0}=S_0$. System (2.3) is hyperbolic and can be integrated by the grid-characteristic method.

Microvasculature in this model is represented by the virtual vessels introduced between terminal arteries and terminal veins. Blood flow in the virtual vessels is also described by the set of equations (2.3).

At junctions of vessels (including virtual ones) the 1D flow satisfies Poiseuille's pressure drop condition (2.5) and the mass balance equation (2.6):

$$\bar{p}_k(S_k(t,\tilde{x}_k))-p^l_{\text{node}}(t)=\varepsilon_k R^l_k S_k(t,\tilde{x}_k)\,\bar{u}_k(t,\tilde{x}_k),\ k=k_1,k_2,\ldots,k_M \tag{2.5}$$
$$\sum_{k=k_1,k_2,\ldots,k_M}\varepsilon_k S_k(t,\tilde{x}_k)\,\bar{u}_k(t,\tilde{x}_k)=0. \tag{2.6}$$

Here l is the junction index, k is the vessel index, $k_1,k_2,\ldots,k_M$ and M are the indices and the number of the vessels meeting at the junction, $p^l_{\text{node}}(t)$ is the pressure at junction l, R^l_k is the hydraulic resistance for the flow from the kth vessel to the lth junction. We set $\varepsilon_k=1$, $\tilde{x}_k=L_k$ for vessels incoming into a junction and $\varepsilon_k=-1$, $\tilde{x}_k=0$ for outgoing vessels. The flow rate $Q=S(t,x)\,\bar{u}(t,x)$ is given at the inlet of the vascular network. Boundary conditions on inlet/outlets and in every vessel junction (2.5)–(2.6) are supplemented with compatibility conditions for the hyperbolic equations (2.3). The 1D model accounts for the presence of venous valves and autoregulation. For details on 1D model implementation we refer to [17, 18, 23].

The 1D and 3D blood flow models are coupled via equations representing continuity of the fluid flux and the continuity of the normal stress. An iterative method is applied to meet these two conditions [5].

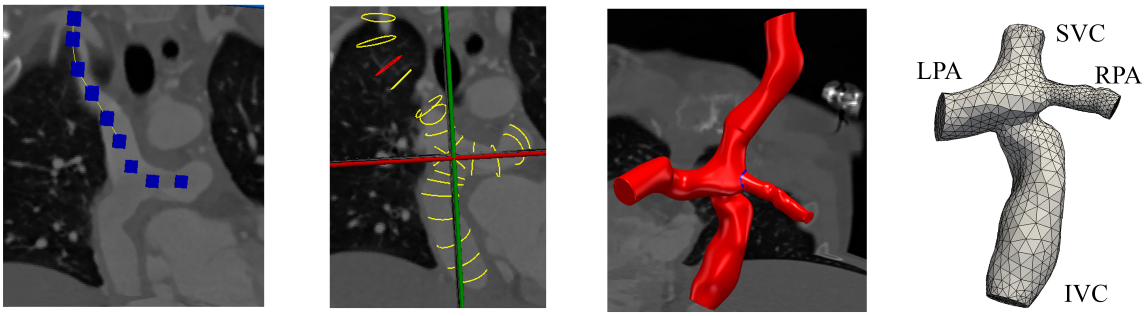

Fig. 2: Discretization of TCPC region: (a) highlighting of centerline; (b) contours of vessels along centerlines; (c) TCPC surface; (d) tetrahedral mesh for TCPC.

3 Patient-specific two-scale blood flow model

Personalization of the two-scale haemodynamic model is achieved via patient-specific geometry, parameters, boundary conditions for the aortic inlet of the 1D model and the TCPC outlets of the 3D model.

3.1 Patient-specific computational domains

Processing of the CT image provides the 3D computational domain involving LPA, RPA, SVC, IVC via the following steps. First, centerlines of the vessels are produced by connecting centers of cross-sections along LPA, RPA, SVC, IVC (see Fig. 2a). Second, contours of each vessel in its cross-sections are defined along every centerline (see Fig. 2b). Third, a surface is spanned over these contours (see Fig. 2c). Forth, a tetrahedral mesh in the domain bounded by the surface is generated. These steps were performed using the SimVascular software package [22]. Mesh cosmetics operations from the Ani3D software package [25] end up with an unstructured tetrahedral mesh with 15481 tetrahedra in the 3D TCPC domain (see Fig. 2d).

The systemic vascular tree (the computational domain for the 1D haemodynamic model) can not be personalized by segmentation of CT or MRI data since the latter is available for the thoracic region only. We adopt a statistically averaged systemic arterial tree for an adult male [17] (see Fig. 3a). Since the patient is a 14 years old male, his height is likely the same as that of a statistically averaged adult male, and no scaling of vessels lengths is needed. The diameters of patient's arteries are equal to the diameters of the averaged adult arteries scaled by factor 0.75 since the time-averaged diameter of patient's aorta recovered from the 4D flow MRI data is 75 % of that for the averaged adult. The venous tree of the systemic circulation is chosen to be symmetric to the arterial tree except for the structure of the aorta and the TCPC (see Fig. 3b). The diameters of patient's veins are set to be 25% larger than the diameters of the corresponding arteries. Such scaling factor reproduces the time-averaged diameters of patient's SVC and IVC recovered from 4D flow MRI data.

3.2 Patient-specific parameters

The venous pressure is assumed to be equal to 5 mmHg (the time-averaged pressure in the right atrium of a healthy adolescent), whereas the systolic and diastolic arterial pressures at the patient's arm should be equal to 110 and 70 mmHg, respectively, and the time-averaged pressure should be 100 mmHg.

The hydrodynamic resistances R_k^l at vessels junctions (2.5) influence the pressure distribution across the vascular tree. The microcirculation resistance parameters $R_{k^*}^l$ (k^* corresponds to the virtual vessel) affect the average pressure in the arteries, the regional blood supply, and the arterio-venous pressure drop. The resistances at vessels junctions range between 1 and 100 dyne·sec/cm^5. They were adjusted to fit blood flow

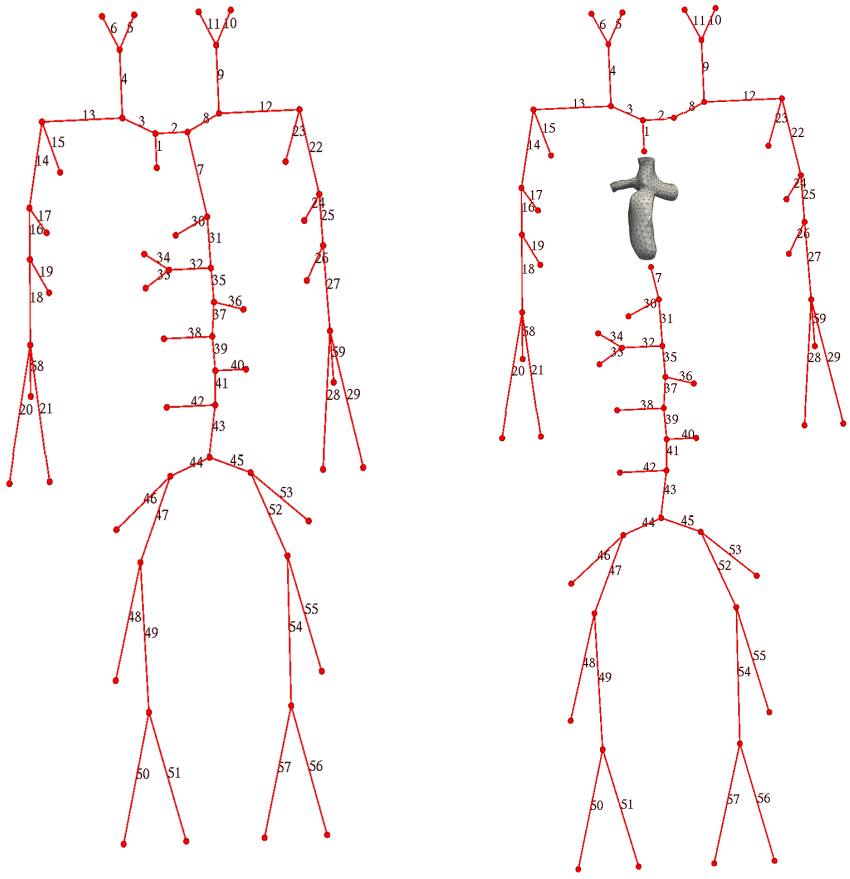

(a) (b)

Fig. 3: 1D vascular network: (a) systemic arteries; (b) systemic veins.

rates and pressures known at several points of the arterial tree for a statistically averaged adolescent male [23]. The microcirculation resistances $R^l_{k^*}$=5660 dyne·sec/cm^5 were set in order to fit the time-averaged pressure at the patient's arm.

Vessel wall elasticity within the 1D haemodynamic model (2.3) is characterized by the velocity of pulse wave propagation c_w. This parameter influences the pressure waveform amplitude, varies in different vessels and depends on patient's age, gender, medical and lifestyle conditions [9, 23]. In the present work we assume that the parameter c_w may have two patient-specific values corresponding to arteries-averaged velocity $c_{w,a}$ and veins-averaged velocity $c_{w,v}$. The velocity of the pulse wave propagation for the virtual vessels (representing arterio-venous coupling) c_{k^*} = 200 cm/sec and the veins-averaged velocity $c_{w,v}$ = 350 cm/sec were chosen to fit haemodynamics of a statistically averaged adolescent male. The arteries-averaged velocity $c_{w,a}$ = 650 cm/sec fits the simulated pressure to the ranges of the pressure waveform at the patient's arm.

Finally, the microcirculation resistances $R^l_{k^*}$ were scaled by two factors $\alpha_{\text{up}} = 1.125$ or $\alpha_{\text{low}} = 0.875$ according to the region of the arterio-venous junction: the factors should provide the patient-specific fraction of the blood flow to the lower limbs which is known from 4D flow MRI data. This fraction may be estimated from two independent data, the time-averaged flow rates in the superior Q_{SVC} and inferior Q_{IVC} vena cava, and the time-averaged flow rates in the two cross-sections of the aorta Q^7_{Aorta} and Q^4_{Aorta} (see Table 1). Both estimates provide the same fraction 0.55.

The above personalization strategy (1D vascular tree calibration and parameter tuning) does not reproduce patient-specific haemodynamics to the full extent. However, based on a few parameters it represents

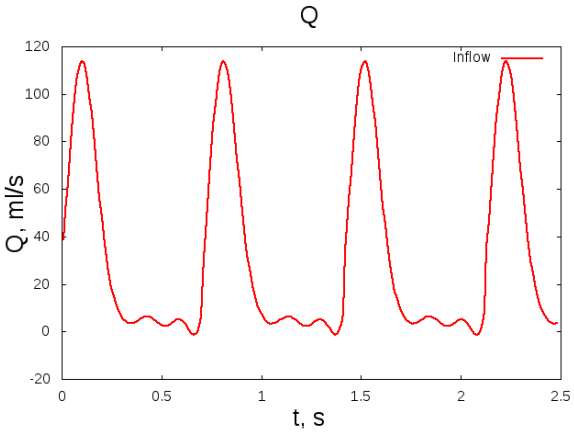

Fig. 4: Inflow rate in aorta.

Q_{in}	RPA	LPA
$0.6Q_{in}$	58%	42%
$0.8Q_{in}$	55%	45%
$1.0Q_{in}$	53%	47%
$1.2Q_{in}$	50%	50%
$1.4Q_{in}$	49%	51%

Tab. 2: Blood flow distribution between RPA and LPA depending on the inflow rate, $R_{RPA} = 90$ dyne·sec/cm^5 and $R_{LPA} = 321$ dyne·sec/cm^5.

basic features of patient's haemodynamics and may be refined further provided a wider set of patient's data. A more advanced technique for parameters estimation uses a linear optimization algoritm [7].

3.3 Boundary conditions for 1D3D haemodynamic problem

The boundary of 3D TCPC domain contains two inlets (SVC and IVC) and two outlets (LPA and RPA). To identify parameters of outflow boundary conditions, we impose constant flow rates Q_{SVC} and Q_{IVC} from Table 1 with parabolic profiles on the inlets.

The outflow boundary conditions may be based on different concepts: coupling with lumped parameter models [3, 10, 14, 20], morphometry-based impedance [13, 19], Poiseuille's pressure drop [23]. In this work we adopt the latter condition in terms of equation (2.2), where p_{out} is the pressure at the pulmonary microvascular bed, initially set to 7 mmHg.

The resistances R_{RPA} and R_{LPA} for each outflow boundary are computed based on known distribution of the time-averaged flow to RPA and LPA (see Table 1): LPA adopts 47% of blood and RPA adopts 53% of blood. The resistances are found iteratively. Setting $R^0_{RPA} = R^0_{LPA} = 138$ dyne·sec/cm^5, we solve the Navier-Stokes equations (2.1) in the TCPC domain with the outlet condition (2.2) and obtain averaged pressures P^n_{RPA} and P^n_{LPA} which contribute to the update of the resistances

$$R^{n+1}_{RPA} = (P^n_{RPA} - p_{out}) \Big/ (0.53Q_{SVC} + 0.53Q_{IVC}), \qquad R^{n+1}_{LPA} = (P^n_{LPA} - p_{out}) \Big/ (0.47Q_{SVC} + 0.47Q_{IVC}).$$

The converged resistances are $R_{RPA} = 90$ dyne·sec/cm^5, $R_{LPA} = 321$ dyne·sec/cm^5.

We note that according to (2.1), (2.2), for fixed resistances the blood flow distribution between RPA and LPA is sensitive to the total inflow rate $Q_{in} = Q_{SVC} + Q_{IVC}$ (see Table 2). This means that the correct total inflow for TCPC is the crucial parameter for estimation of the resistances R_{RPA} and R_{LPA}. In order to provide the time-averaged aortic flow rate equal to Q_{in}, we scale the MRI-based time-dependent inflow aortic flow waveform in the aortic cross-section 4 (see Fig. 1a) by the constant Q_{in}/Q_{aorta}. The scaled flow rate waveform in the aorta shown in Fig. 4 serves as the inflow boundary condition for the 1D3D haemodynamic model.

3.4 Computation of a quasi-stationary regime in the two-scale blood flow model

As it was mentioned in Section 1, the actual blood pressure in TCPC for Fontan patients is almost constant in time. Therefore, computation and postprocessing of a quasi-stationary regime in the two-scale blood flow model provides feasible flow metrics. Since the 1D haemodynamic model includes tens of elastic vessels, it takes significant number of cardiac cycles to achieve a quasi-stationary regime. On the other hand, the 1D model is computationally cheaper than the 3D flow model in TCPC. The following iterative algorithm reduces the computational time for achieving the quasi-stationary regime in TCPC. The number of iterations does not exceed 5. On input it takes catheter-measured or expected pressure P_{ref} at a point of TCPC (14 mmHg in case of our patient). The algorithm outputs the pulmonary pressure $p_{\text{out}} = 10.5$ mmHg makes the computed pressure P_{TCPC} equal to the expected pressure P_{ref} at the same point of TCPC.

Algorithm 1

Require: Measured or expected pressure P_{ref} in TCPC domain

1: Run the 1D model of the systemic circulation with outflow pressure $P^{1D}_{\text{outflow}} = 5$ mmHg until the quasi-stationary regime in the TCPC region is established
2: Run the 1D3D model for several cardiac cycles, the 1D part is initialized by the solution from Step 1. Evaluate quasi-stationary pressure P_{TCPC}, cross-section-averaged pressures P_{SVC}, P_{IVC} until a quasi-stationary regime in the 1D3D model is established
3: Update pressures so that P_{TCPC} matches P_{ref}:

$$p_{\text{out}} := p_{\text{out}} + P_{\text{ref}} - P_{\text{TCPC}}, \quad P^1_{\text{SVC}} = P_{\text{SVC}} + P_{\text{ref}} - P_{\text{TCPC}}, \quad P^1_{\text{IVC}} = P_{\text{IVC}} + P_{\text{ref}} - P_{\text{TCPC}}$$

4: Set $i = 1$
5: **repeat** ▷ iteration
6: Run the 1D model of the systemic circulation with outflow pressures P^i_{SVC}, P^i_{IVC} until the quasi-stationary regime in the TCPC region is established
7: Run the 1D3D model for several cardiac cycles with outflow pressure p_{out}, the 1D part being initialized by the solution from Step 6
8: Set $P^{i+1}_{\text{SVC}} = P_{\text{SVC}}$, $P^{i+1}_{\text{IVC}} = P_{\text{IVC}}$
9: $i := i + 1$
10: **until** quasi-stationary regime in 1D3D model is established
11: **if** $|P_{\text{ref}} - P_{\text{TCPC}}|$ is not small **then goto** Step 3
12: **end if**

4 Haemodynamics of the Fontan patient

The two-scale haemodynamic model was tuned for the anonymized Fontan patient in horizontal position and then applied to the same patient in standing position. Simulation of standing haemodynamics accounts for the gravity force, the autoregulation (ignored in horizontal position) and the venous valves (inactive in horizontal position), for details we refer to [23]. The analysis of haemodynamics in these positions is important for diagnostics and prediction of operation outcomes such as exercise intolerance of Fontan patients.

Table 3 collects time-averaged pressures and flow rates on TCPC inlets (IVC, SVC) and outlets (RPA, LPA) computed in both positions.

For horizontal position, the distribution of computed time-averaged flow rates in IVC, SVC, RPA, LPA from Table 3a match the 4D flow MRI data shown in Table 1, and the computed pressure in TCPC is close to 14 mmHg (the expected pressure P_{ref}). The computed flow in TCPC is weakly pulsatile, its pulsation is smaller than 4D flow MRI data. The basic reason for the weakly pulsatile flow is the constant pressure p_{out} in the Poiseuille's outflow boundary condition (2.2). On the other hand, the catheter-based pressure measurements in TCPC demonstrate almost non-pulsatile flow, and the choice of (2.2) seems to be feasible. The pressure field and

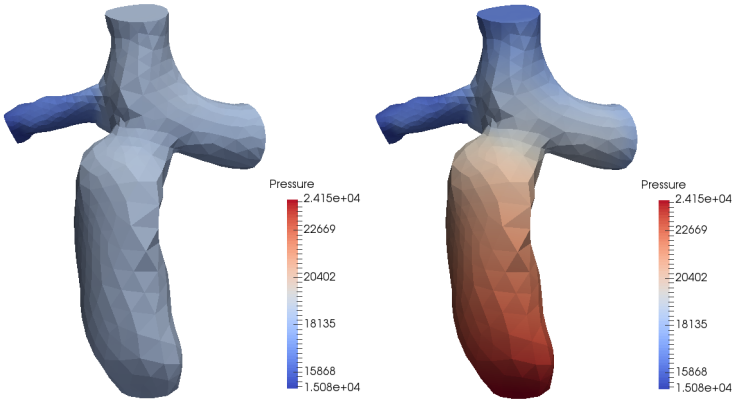

(a) (b)

Fig. 5: Pressure field in TCPC for the Fontan patient in horizontal (a) and standing (b) positions.

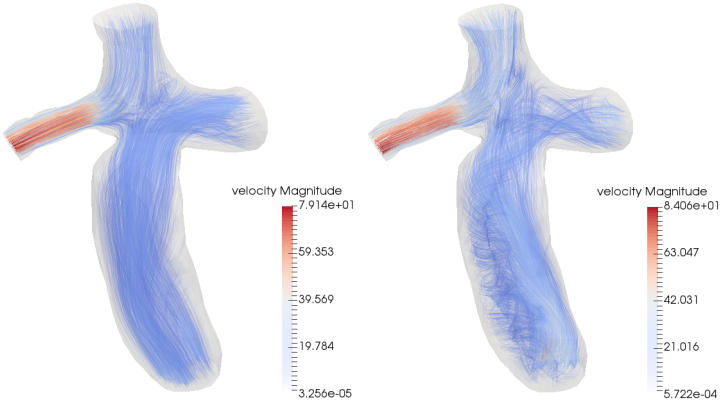

(a) (b)

Fig. 6: Velocity streamlines in TCPC for the Fontan patient in horizontal (a) and standing (b) positions.

velocity streamlines in TCPC are shown in Figs. 5a and 6a, respectively. The computed velocity streamlines are similar to those reproduced in the 4D flow MRI measurement (see Fig. 1c) and indicate that most blood from IVC flows to LPA and from SVC flows to RPA without mixing.

For standing position, 4D flow MRI data are not available and verification of the computed values of interest is not possible. The model demonstrates considerable change of blood flow distribution between upper and lower limbs, Q_{SVC} and Q_{IVC}, respectively: the time-averaged flow increases in the upper body and decreases in the lower body (see Table 3b). The distribution between RPA and LPA is also changed: the time-averaged flow decreases in the left lung and increases in the right lung. Incorporation of the 1D haemodynamic model makes it possible to estimate the impact of the patient's position on the regional flow rates. The pressure field (see Fig. 5b) and the velocity streamlines (see Fig. 6b) in TCPC illustrate the above observations: the pressure increases from SVC towards IVC and the intraflows IVC-LPA and SVC-RPA mix to a greater extent due to the helical velocity field in IVC.

Comparison of other haemodynamic indices in horizontal and standing positions shows that most of them become worse in standing position: the central venous pressure in IVC is higher by 4 mmHg, the hepatic blood flow is less intensive (0.53), the flow distribution between RPA and LPA is more unbalanced (see Table 3). Moreover, the energy efficiency of TCPC reduces from 95% in horizontal position to 84% in standing position due to generation of vortexes. The energy efficiency is the ratio of flow energies at the outflow and inflow boundaries of TCPC. The pressure range in the descending aorta is [82.2:117.7] mmHg for horizontal

Tab. 3: Time-averaged pressures P_{av} (mmHg) and flow rates Q_{av} (ml/sec) on TCPC inlets and outlets for the Fontan patient in horizontal (a) and standing (b) positions. $Q_{in} = Q_{IVC} + Q_{SVC}$ is the time-averaged inflow rate for TCPC.

(a) Horizontal position				(b) Standing position			
Vessel name	P_{av} (mmHg)	Q_{av} (mL/sec)	Q_{av}/Q_{in}	Vessel name	P_{av} (mmHg)	Q_{av} (mL/sec)	Q_{av}/Q_{in}
IVC	13.90	15.88	55.0%	IVC	17.93	15.18	52.8%
SVC	13.88	13.01	45.0%	SVC	12.31	13.59	47.2%
LPA	13.77	13.59	47.0%	LPA	13.57	12.81	44.5%
RPA	11.53	15.30	53.0%	RPA	11.57	15.96	55.5%

position and [81.2:121.2] mmHg in standing position. The pressure gradient between the descending aorta and IVC is [68.3:103.8] mmHg in horizontal position and [63.3:103.3] mmHg in standing positions. Thus the pressure gradient between the hepatic arteries and veins in standing position is smaller and hepatic blood flow should be less intensive.

Therefore, in standing position blood flow of Fontan patients becomes more hampered that correlates with their exercise intolerance.

5 Conclusions

We presented the two-scale (1D3D) haemodynamic model of the systemic circulation for a patient who has underwent Fontan surgical operation. Personalization of the model exploits CT data for reconstruction of TCPC region, 4D flow MRI and anthropometric data for scaling of the population-averaged 1D vascular tree, 4D flow MRI data for inflow and outflow boundary conditions. Catheterized pressure and/or ultrasound measurements can enrich personalization of the model. In spite of attractivity, the 4D flow MRI data should be used with great caution as they are prone to significant noise. In our model we use MRI-based flow rate in the aorta cross-section only as they have acceptable 15% noise. MRI-based time-averaged flow rates on inlets and outlets of TCPC are used for scaling of the aortic flow and tuning the resistances of the pulmonary microvasculature bed. Time-averaging reduces the noise of the measurements.

The 1D3D model is tuned to patient's data and is able to reproduce measured time-averaged flow rates at the inlets and outlets of TCPC, as well as measured or expected pressure in TCPC for the patient in horizontal position. The model provides regional (TCPC) and global haemodynamics of the patient in standing position as well. Most of haemodynamic indices indicate that the blood flow becomes hampered in standing position confirming clinically known exercise intolerance of Fontan patients.

The presented model has limitations. Comparison of blood flows passing through the lungs requires incorporation of the 1D haemodynamic model of the pulmonary circulation. The simplest Poiseuille's outflow boundary condition (2.2) and the constant outflow pressure p_{out} make the TCPC flow almost non-pulsatile. Although the non-pulsatility does not contradict catheterized pressure measurements, 4D flow MRI data indicate the flow pulsatility. Other types of boundary conditions will be studied in the future research.

The 1D3D model is important for the computational study of the Fontan circulation and prediction of the Fontan surgical operations as it can take into account different pathologies and physiological effects including physical activities, similarly to the approach [17].

Acknowledgment: The authors thank Ksenia Slepova for her assistance in the TCPC domain segmentation and 3D mesh generation.

Funding: The study was performed at Marchuk Institute of Numerical Mathematics RAS and supported by the Russian Science Foundation (project 21-71-30023).

References

[1] A. Baretta, C. Corsini, W. Yang, I. E. Vignon-Clementel, A. L. Marsden, J. A. Feinstein, T. Y. Hsia, G. Dubini, F. Migliavacca, and G. Pennati, Modelling of Congenital Hearts Alliance (MOCHA) investigators. Virtual surgeries in patients with congenital heart disease: a multi-scale modelling test case. *Philos. Trans. A Math. Phys. Engrg. Sci.* **369** (2011), 4316–4330.

[2] C. Bertoglio, R. Nuñez, F. Galarce, et al., Relative pressure estimation from velocity measurements in blood flows: State-of-the-art and new approaches. *Inter. J. Numer. Meth. Biomed. Engrg.* **34** (2017), No. 2, e2925.

[3] C. Corsini, C. Baker, E. Kung, S. Schievano, G. Arbia, A. Baretta, G. Biglino, F. Migliavacca, G. Dubini, G. Pennati, A. Marsden, I. Vignon-Clementel, A. Taylor, T. Y. Hsia, and A. Dorfman, Modeling of Congenital Hearts Alliance (MOCHA) Investigators. An integrated approach to patient-specific predictive modeling for single ventricle heart palliation. *Comput. Meth. Biomech. Biomed. Engrg.* **17** (2014), No. 14, 1572–1589.

[4] K. Desai, C. M. Haggerty, K. R. Kanter, et al., Haemodynamic comparison of a novel flow-divider Optiflo geometry and a traditional total cavopulmonary connection. *Interact. Cardiovasc. Thorac. Surg.* **17** (2013), No. 1, 1–7.

[5] T. Dobroserdova, M. Olshanskii, and S. Simakov, Multiscale coupling of compliant and rigid walls blood flow models. *Int. J. Numer. Meth. Fluids* **82** (2016), No. 12, 799–817.

[6] P. Dyverfeldt, M. Bissell, A. J. Barker, et al., 4D flow cardiovascular magnetic resonance consensus statement. *J. Cardiovasc. Magn. Reson* **17** (2015), No. 1, 1–19.

[7] T. Gamilov, J. Alastruey, and S. Simakov, Linear optimization algorithm for 1D hemodynamics parameter estimation. In: *Proc. of the 6th European Conference on Computational Mechanics: Solids, Structures and Coupled Problems, ECCM 2018 and 7th European Conference on Computational Fluid Dynamics, ECFD 2018*. 2020, pp. 1845–1850.

[8] A. M. Ismailbaev and T. O. Astrakhantseva, Late results of the extracardiac Fontan procedure. *Bulletin A. N. Bakuleva NMRCCS RAMS* **15** (2014), No. 6.

[9] E. S. J. Krner, H. J. Lamb, H.-M. J. Siebelink, S. C. Cannegieter, P. J. Van Den Boogaard, E. E. Van Der Wall, A. De Roos, and J. J. M. Westenberg, Pulse wave velocity and flow in the carotid artery versus the aortic arch: effects of aging. *J. Magn. Reson. Imaging* **40** (2014), No. 2, 287–293.

[10] J. Liu, W. Yang, I. S. Lan, and A. L. Marsden, Fluid-structure interaction modeling of blood flow in the pulmonary arteries using the unified continuum and variational multiscale formulation. *Mechanics Research Communications* **107** (2020).

[11] A. L. Marsden, A. J. Bernstein, V. M. Reddy, S. C. Shadden, R. L. Spilker, F. P. Chan, C. A. Taylor, and J. A. Feinstein, Evaluation of a novel Y-shaped extracardiac Fontan baffle using computational fluid dynamics. *J. Thorac. Cardiovasc. Surg.* **137** (2009), No. 2, 394–403.e2.

[12] F. Migliavacca, R. Balossino, G. Pennati, G. Dubini, T. Y. Hsia, M. R. de Leval, E. L. Bove, Multiscale modelling in biofluidynamics: application to reconstructive paediatric cardiac surgery. *J. Biomech.* **39** (2006), No. 6, 1010–1020.

[13] M. Monjezi, M. Ghoreyshi, M. S. Saidi, M. A. N. Navabi, and B. D. Firoozabadi, 3D-1D Simulation of Flow in Fontan Operation: Effects of Antegrade Flow on Flow Pulsations. *Scientia Iranica* **21** (2014), No. 4, 1378–1389.

[14] G. Pennati, C. Corsini, D. Cosentino, T. Y. Hsia, V. S. Luisi, G. Dubini, and F. Migliavacca, Boundary conditions of patient-specific fluid dynamics modelling of cavopulmonary connections: possible adaptation of pulmonary resistances results in a critical issue for a virtual surgical planning. *Interface Focus* **1** (2011), No. 3, 297–307.

[15] V. P. Podzolkov, Actual problems of surgical treatment of congenital heart diseases with univen-tricular hemodynamics by the Fontan procedure. *Bakoulev J. Cardiovasc. Diseases* **19** (2018), No. 5, 625–636.

[16] S. Simakov and A. Kholodov, Computational study of oxygen concentration in human blood under low frequency disturbances. *Mathematical Models and Computer Simulations* **1** (2009), No. 2, 283–295.

[17] S. Simakov, T. Gamilov, and Y. N. Soe, Computational study of blood flow in lower extremities under intense physical load. *Russ. J. Numer. Anal. Math. Modelling* **28** (2013), No. 5, 485–504.

[18] S. Simakov, Spatially averaged haemodynamic models for different parts of cardiovascular system. *Russ. J. Numer. Anal. Math. Modelling* **35** (2020), No. 5, 285–294.

[19] R. L. Spilker, J. A. Feinstein, D. W. Parker, V. M. Reddy, and C. A. Taylor, Morphometry-based impedance boundary conditions for patient-specific modeling of blood flow in pulmonary arteries. *Ann. Biomed. Engrg.* **35** (2007), No. 4, 546–559.

[20] G. Troianowski, C. A. Taylor, J. A. Feinstein, and I. E. Vignon-Clementel, Three-dimensional simulations in Glenn patients: clinically based boundary conditions, hemodynamic results and sensitivity to input data. *J. Biomech. Engrg.* **133** (2011), No. 11, 111006.

[21] P. M. Trusty, T. C. Slesnick, Z. A. Wei, et al., Fontan surgical planning: Previous accomplishments, current challenges, and future directions. *J. Cardiovasc. Trans. Res.* **11** (2018), 133–144.

[22] A. Updegrove, N. M. Wilson, J. Merkow, H. Lan, A. L. Marsden, and S. C. Shadden, SimVascular: an open source pipeline for cardiovascular simulation. *Ann. Biomed. Engrg.* **45** (2017), No. 3, 525–541.

[23] Yu. Vassilevski, M. Olshanskii, S. Simakov, A. Kolobov, and A. Danilov, *Personalized Computational Hemodynamics. Models, Methods, and Applications for Vascular Surgery and Antitumor Therapy*. Academic Press, 2020.

[24] D. A. de Zelicourt and V. Kurtcuoglu, Patient-specific surgical planning, where do we stand? The example of the Fontan procedure. *Ann. Biomed. Engrg.* **44** (2016), 174–186.

[25] *Advanced Numerical Instruments in 3D*. https://sourceforge.net/projects/ani3d/